AerospaceEurope Conference2020
BORDEAUX, FRANCE | 25 - 28 FEBRUARY 2020
CEAS Council of European Aerospace Societies
HOSTED BY: 3AF Association Aéronautique et Astronautique de France

COMMON NUMERICAL METHODS & COMMON EXPERIMENTAL MEANS FOR THE DEMONSTRATORS OF THE LARGE PASSENGER AIRCRAFT PLATFORMS

Wolf R. Krüger [(1)], Fritz Boden [(2)], Tania Kirmse [(2)], Jonathan Lemarechal [(2)], Andreas Schröder [(2)], Hans Peter Barth [(2)], Sebastian Oertwig [(3)], Henri Siller [(3)], Jan Delfs [(4)], Antoine Moreau [(3)], Dominik Schäfer [(1)], Arne Stürmer [(4)], Marco Norambuena [(1)]

DLR - German Aerospace Center
(1) Institute of Aeroelasticity, Bunsenstr. 10, 37073 Göttingen, Germany,
Email: Wolf.Krueger@DLR.de, D.Schaefer@DLR.de, Marco.Norambuena@DLR.de
(2) Institute of Aerodynamics and Flow Technology, Bunsenstr. 10, 37073 Göttingen, Germany,
Email: Fritz.Boden@DLR.de, Tania.Kirmse@DLR.de, Jonathan.Lemarechal@DLR.de, Andreas.Schroeder@DLR.de, Peter.Barth@DLR.de
(3) Institute of Propulsion Technology, Department of Engine Acoustics, Müller-Breslau-Str.8, 10623 Berlin, Germany, Email: Sebastian.Oertwig@DLR.de, Henri.Siller@DLR.de, Antoine.Moreau@DLR.de
(4) Institute of Aerodynamics and Flow Technology, Lilienthalplatz 7, 38108 Braunschweig, Germany
Email: Arne.Stuermer@DLR.de, Jan.Delfs@DLR.de

KEYWORDS: Numerical simulation methods, aeroacoustic calculations and measurements, parametric modelling, aeroelastic stability, Shake-the-Box, deformation measurements, IPCT, propulsion, Clean Sky, TSP, crossflow instability, active excitation control, vibroacoustics

ABSTRACT:

The integration of advanced propulsion systems into the aircraft, and the assessment of their benefits related to e.g. fuel burn, noise emission and potential further measures, is one of the major activities of the Large Passenger Aircraft (LPA) Platform 1 of the Clean Sky 2 initiative. In order to optimize and assess the potential of advanced propulsion integration, it is necessary to establish suitable design, evaluation, and measurement tools. The so-called Cross-Demonstrator-Capabilities (XDC-) activities have been set up to develop and demonstrate powerful numerical and experimental methods for aerodynamic, aeroacoustics and aeroelastic simulation and measurement tasks, supporting the dedicated demonstrators of LPA. The paper will give an overview of the XDC activities and some examples of the developments related to this demonstrator.

1. Introduction

With respect to the Clean Sky 2 objectives to reduce CO_2 and noise emissions, the Large Passenger Aircraft (LPA) Platform 1 aims to develop and integrate advanced propulsion systems. This effort requires suitable tools for the prediction, optimization, and the evaluation of new technologies as well as for validation testing in the technical disciplines shown in Fig. 1. Thus, within LPA Platform 1 the XDC is used to develop and demonstrate numerical and experimental means for the integration of advanced propulsion systems (e.g. Ultra High Bypass Ratio (UHBR) engines, Open Rotor (OR) propulsion or Boundary Layer Ingestion (BLI)) and to assess and verify the related benefits (e.g. on fuel burn and noise). The main objective of the XDC is to establish advanced design processes and tools that are applicable to the LPA Platform 1 propulsion systems. The development is divided into two fields: common numerical methods and common experimental means, both adressing aerodynamics, vibro-acoustics, aeroacoustics and aeroelasticity.

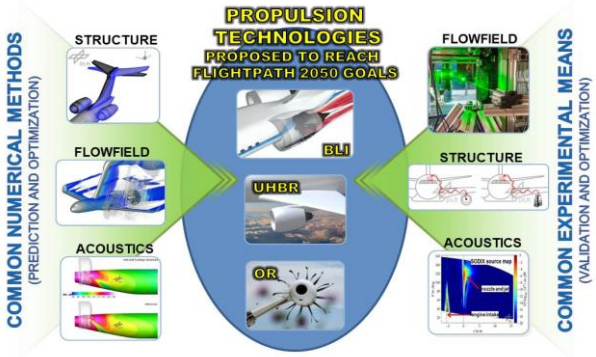

Figure 1: Means required for the assessment of novel propulsion technologies.

2. Common Numerical Methods

The work on common numerical methods is divided into three main branches:

- numerical aerodynamic simulation methods,
- numerical aeroacoustic calculations and noise predictions,
- aeroelastic modelling and stability analysis.

Examples of the activities in these main branches are briefly presented in the following.

2.1. Numerical Aerodynamic Simulations

The engine-airframe configurations of primary

interest in the LPA studies in Platform 1 all feature a very close coupling, if not even full integration, of the aircraft and the propulsion system. Future aircraft are expected to use ever higher bypass ratio engines, which will require a very tight integration on and with the wings of the aircraft due to the large engine nacelle diameters. Even more mutual interactions between the airframe and the propulsion system will occur for another promising technology development utilizing boundary layer ingesting (BLI) engines, where shrouded fan systems are likely to be integrated on or around the empennage or tailcone of the aircraft. Thus, in order to be able to obtain accurate aerodynamic performance predictions, Computational Fluid Dynamics (CFD) studies of the overall aircraft necessitate an adequate level of fidelity in the modelling of the engine, as well as the mutual interaction between the airframe and the propulsion system. While some recent developments of simplified models of turbofan engine fan systems in the form of actuator disc or body force approaches appear promising, the highest fidelity approach which would reliably account for all important aerodynamic interactions between the engine and airframe is the full geometric modelling of the fan stage in a fully unsteady RANS-based analysis of the aircraft [1-6]. An additional advantage of this expensive simulation approach is its ability to deliver unsteady near-field pressure data in the engine proximity, which may be very valuable for subsequent aeroacoustic studies.

To understand the best modelling approaches for the engine fan module available in the DLR-developed TAU-Code, a comparison of a classical engine boundary condition and a high-fidelity rotating fan unsteady approach has been done in the frame of the Clean Sky 2 project based on a generic isolated UHBR engine configuration. The uRANS modelling method developed using these simpler isolated engine studies are expected to be directly applicable to future complex integrated engine–airframe configuration studies, including the challenging BLI-engine-airframe cases [7].

Figure 2: ASPIRE isolated UHBR turbofan (geometry not to scale).

The isolated UHBR engine studied in this paper and shown in Fig. 2 was designed within the EU Clean Sky 2 research project ASPIRE as a generic engine for numerical studies and is representative of a modern UHBR turbofan [1,2,8]. The nacelle, a very aggressive design with a small length-to-diameter ratio to minimize the external surface area, was supplied by Airbus, while the fan stage, designed for application in a geared turbofan type engine with a low pressure ratio and a 16:1 bypass ratio, was designed by the DLR Institute of Propulsion Technology. The uRANS investigations have focused on four engine operating point (Sideline, Buzz-Saw Noise, Cutback and Approach), which are reference points for the noise certification of an aircraft.

All CFD simulations are performed utilizing the DLR TAU-Code, while a family of 4-block Chimera grid using hybrid-unstructured CentaurSoft Centaur as well as fully block-structured ICEMCFD Hexa meshes with up to 200 x 106 nodes is used.

Table 1 lists selected mean aerodynamic performance results achieved in the DLR TAU uRANS simulations. For all studied operating points, the results for the fan mass flow and the fan stage pressure ratio are listed as deviations from the engine model specifications. While the challenging low fan pressure ratio APP case shows an offset of up to 3% versus the targets, the results for other operating points generally only show deviations on the order of about 1%.

Table 1: Mean aerodynamic fan performance predictions as deviations from the engine specifications for mass flow and fan pressure ratio.

	Fan Massflow	Fan Pressure Ratio
Approach	-2.06%	-1.37%
Sideline	-1.23%	-0.83%
Buzz-Saw Noise	-0.44%	-1.91%
Cutback	-0.236%	-1.14%

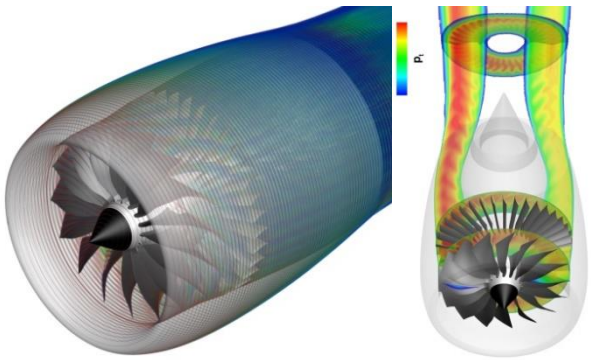

Figure 3: ASPIRE isolated UHBR turbofan uRANS results, showing good resolution of wake and vortices as well as the jet flow non-uniformity resulting from the external aerodynamics influence on the fan for this short intake configuration.

Fig. 3 gives a qualitative impression of the ability of the uRANS simulations on the fine mesh to capture important aerodynamic flow characteristics such as the fan blade wakes and vortices in their interaction with the stator vanes as well as the development of the engine jet. The latter effect is a key feature typical of these short nacelle configurations subject to non-uniform inflow conditions, such as high angles of attack for example. With the fully geometrically modelled fan and OGV an azimuthal variation in the blade and stator loading is the consequence, which also results in a non-axisymmetric jet development, with higher jet total pressures on the right side of the engine than on the left.

While for most applications this degree of fidelity in jet modelling is not a particular concern, there may be cases where the jet and inflow non-uniformity is important. Such cases could be studies of engine jet and wing or high-lift system interactions for closely coupled UHBR engine integrations or also studies of configurations with a boundary layer ingesting integration of the engines. In particular, at the low-speed flight conditions, strong inflow perturbations occur, making a better understanding and modelling of the jet development — as well as a proper modelling of the non-uniform fan face flow — an important issue for external aero-dynamics.

This work has demonstrated the capabilities of the DLR TAU Code to deliver high-accuracy performance predictions as well as detailed insight into the complex aerodynamic flow features representative for the challenges associated with the integration of modern engines with future transport aircraft configurations. In present as well as future work in the frame of Clean Sky 2, these capabilities will be utilized in the analysis of novel aircraft configurations featuring closely coupled UHBR engines in an under-wing integration, as well as with BLI engines mounted on the tailcone, which should allow for in-depth studies on the benefits and challenges these future engine-airframe integration scenarios present.

2.2. Preliminary fan noise design

With the advent of UHBR engines, the question of engine integration has become prominent also in terms of acoustics. Whether the engine is integrated more strongly into the fuselage, or still remains hanging under the wing, the fan of a UHBR engine is likely to experience a less clean inflow due to the boundary layer ingestion (BLI) or due to the short nacelle that is not able to damp the flow distortion induced by the incidence of the engine. The acoustic interaction between the distortion and the fan may represent a risk in terms of noise certification levels.

To address this question early during the design of future engines, a fast analytical tool, called PropNoise, developed by the DLR Institute of Propulsion Technologies, has been extended to the source of tonal self-noise from a supersonic rotor [9] and recently, an experimental validation of this extension has been documented [10]. The impact of an inflow distortion of this source is presented hereafter.

The flow distortion ingested by the fan modifies the strength of the shocks generated by the supersonic rotor blades. As shown in Fig. 4, the presence of inflow distortion triggers the rise of buzz-saw noise at slightly lower Mach number than in the clean-flow case. But the maximum levels are only weakly affected.

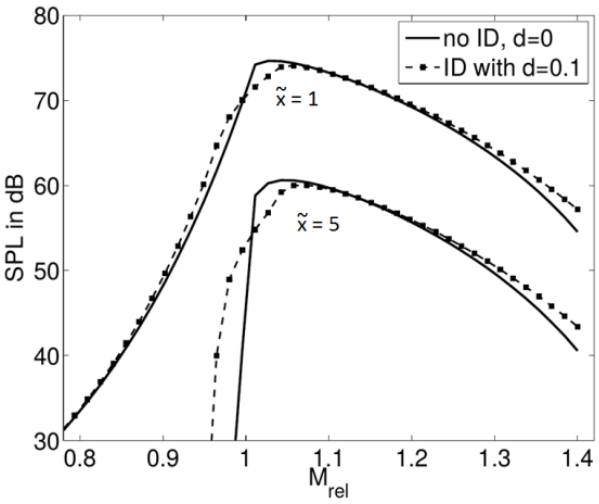

Figure 4: Effect of inflow distortion on average shock strength at two axial positions.

The second impact of inflow distortion is on the propagation of the sound field inside the intake. The circumferential non-homogeneous flow induces a modal scattering, represented in Fig. 4, that tends to weaken the axial decay of the shocks (see in Fig. 5 the r.m.s. value does not decrease anymore for x < 0.4 m). The mechanism underlying this effect is the switch from cut-off to cut-on conditions due to the scattering into low-order modes.

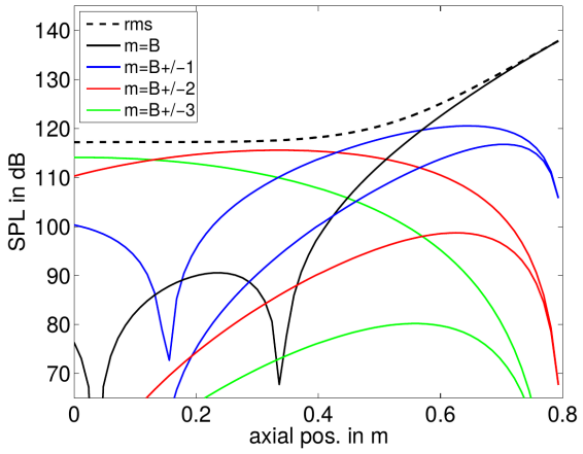

Figure 5: Modal scattering of the blade-passing frequency due to inflow distortion.

As a result of both mechanisms of shock generation and propagation, the emitted sound power is particularly impacted by the inflow distortion in the transonic domain of operation of the fan. It is equivalent to formulate that the buzz-saw noise source may be important at transonic Mach numbers (M_{tr}) where it should be cut-off with clean inflow (see Fig. 6, the region just above M_{tr} = 1 has higher levels with distortion). Therefore the inflow distortion constitutes an acoustic risk, which shall be considered during the design of future UHBR fans and engines.

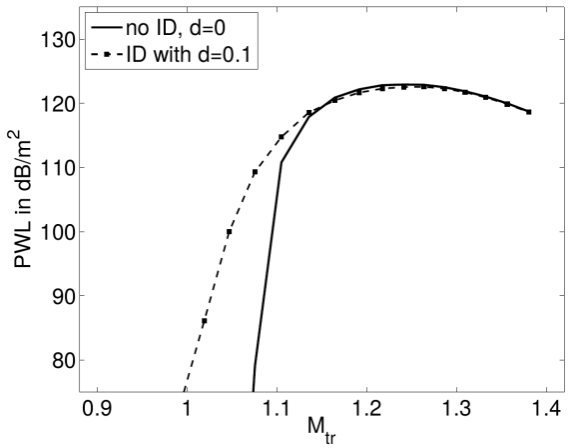

Figure 6: Effect of the inflow distortion of sound power emitted by the fan along a working line.

To conclude, this paragraph has shown that some acoustic aspects of the UHBR engines can be addressed by means of analytical methods, which represent a good alternative for more demanding CFD/CAA simulations. Moreover, at the early design stage, the more simple approach with PropNoise enables to cope with a small amount of information about the engine and fan geometry, whereas more demanding simulations require detailed input not available at the time.

2.3. Aeroelastic Modelling and Analysis

2.3.1. Aeroelastic Model of a Reference Configuration

For the development of numerical methods for aeroelastic analysis and vibration analyses on future aircraft configurations, representative reference models for the aerodynamics and the aircraft structure are necessary. Only very few models with a sufficient level of detail are publicly available.

As the emphasis inside the XDC is on short-range configurations, it was decided to base the aeroelastic reference model on the available, so-called DLR-D150 configuration [12], see Fig. 7. This model of an A320 - size aircraft has been used for flight loads analysis in several DLR and German national (Lufo-) projects. The FEM was, however, lacking a detailed representation of the fuselage. Thus, focus of the work has been the generation of fuselage models of sufficient detail for aeroelastic and vibroacoustic analysis.

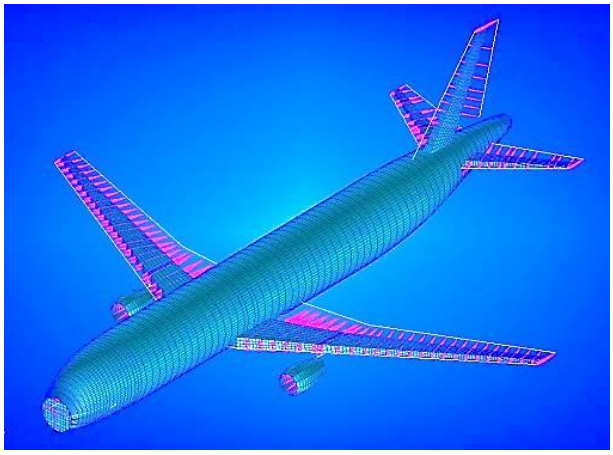

Figure 7: Reference aircraft model

A proper modelling of global mass and stiffness characteristics is a prerequisite for aeroelastic models. The modelling process used by DLR in LPA is MONA [13], consisting of the in-house development ModGen [14] and the commercial finite element software MSC Nastran. Basis of that process is the parametric modelling of wing and fuselage structures, allowing fast variations of design parameters, thus providing a basis for optimization.

Applying the MONA process, three main steps are conducted - the parametric model set-up, followed by an extensive loads analysis campaign, and a structural optimization of the wing structures (this includes the main wings and the tailplane). Aeroelastic requirements like sufficient control surface efficiency are taken into account.

The parametric model set-up within ModGen is based on a parametrically defined geometry of the wing-like components and the fuselage. This comprises the outer geometry generated by the defined airfoils and their position on the wing, and all significant elements of the inner load carrying structure like the spars, ribs and stringers. In addition, ModGen formulates the optimization problem used in the structural sizing step.

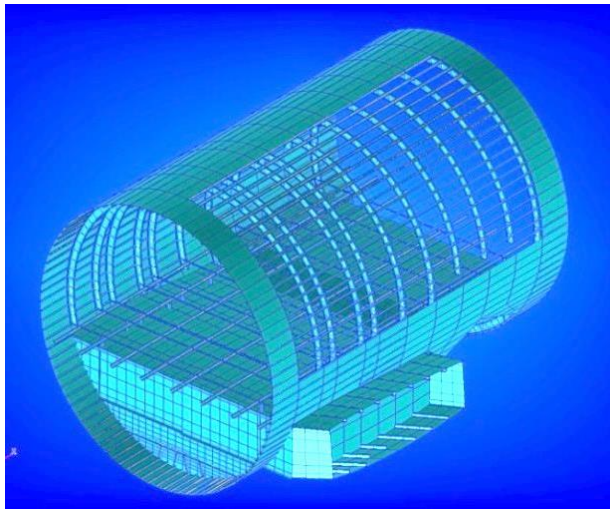

Figure 8: Model of D150 center section.

Nastran is applied in the MONA process for the comprehensive loads analysis and the subsequent structural sizing of the airframe by means of structural optimization.

In the project, a parametric fuselage model was developed. The topology of the fuselage is similar to that of an A320. The dynamics of the aircraft are very much dependent on the interconnection between fuselage and main wings, the so-called center section, shown in Fig. 8.

For the detailed analysis of the rear end, a good representation of the rear fuselage and the vertical and horizontal tail is mandatory. Thus, a detailed topology representation has been developed for the joint between fuselage and empennage (see Fig. 9), including the pressure bulkhead.

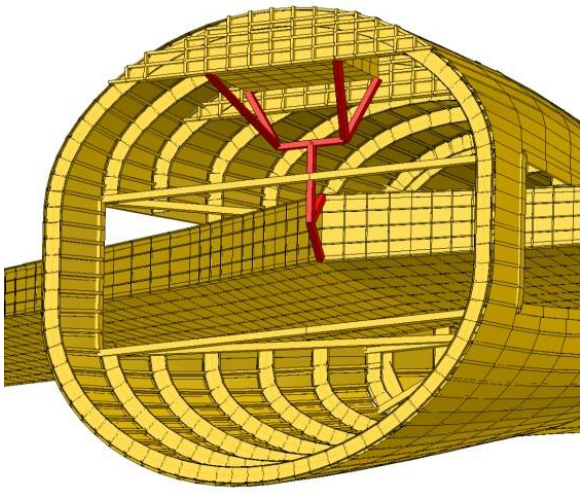

Figure 9: Empennage attachment.

Finally, a full aircraft model is assembled, see Fig. 7. For the representation of the aerodynamics, not required for vibroacoustic analysis but, of course, needed for aeroelastic investigations, the full aircraft model comes with a grid used for potential flow, i.e. Vortex-Lattice- or Doublet-Lattice-(VLM/DLM) aerodynamics. A definition of the coupling between structural model and aerodynamic model is also included.

In a last step, a model suitable for vibroacoustic analysis has been derived. For that purpose, the model has been extended to include more details in those elements essential for vibroacoustic. To ensure the validity of the model for the investigations also performed in the XDC, the MONA model has been compared to a finite element model specifically set-up for vibroacoustic analysis, the so-called FlightLab model, a finite element model of an Airbus A320 fuselage which represents the target level of detail for the vibroacoustic analyses, see Fig. 10.

As a result of the work, now reference models for aeroelastic analysis, loads analysis and vibro-acoustic analysis for engine integration studies are available in the XDC.

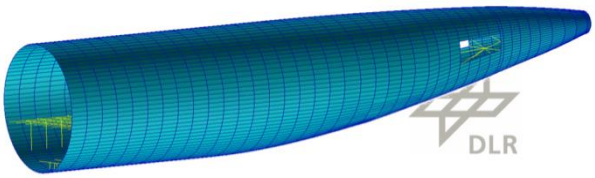

Figure 10: Vibroacoustic model of center section from MONA process

2.3.2. T-Tail Stability Analysis

The conventional approach for flutter predictions heavily relies on the Doublet-Lattice Method (DLM) for computing subsonic unsteady aerodynamic forces. For this, the aerodynamic model is discretized into small trapezoidal elements, which feature two degrees of freedom for generating unsteady aerodynamic forces, namely vertical translation (plunge) and rotation around the lateral axis (pitch). Aerodynamic forces induced by longitudinal and lateral displacements as well as rotations around the longitudinal and vertical axes are not considered and, hence, are assumed to be negligible for the flutter onset. In addition, the steady state aerodynamic forces are assumed to have no effect on the flutter onset either and ignored as well.

In the aeroelastic community, it is well known that T-tail designs (like shown in Fig. 11) feature adverse flutter characteristics which strongly depend on aerodynamic forces induced by inplane and roll deformations of the horizontal tail plane (HTP) along with the steady aerodynamic trim forces [15-19]. This dependency is introduced by the HTP being mounted on the flexible vertical tail plane (VTP) and can also be assumed to be relevant for H-tail configurations, where the VTPs are mounted at the tip of the HTP. It is therefore necessary to account for these additional aerodynamic forces in the flutter prediction of T- and H-tail configurations. Measures for this include corrections of DLM results by external methods, extensions of the DLM for the lacking degrees of freedom, unsteady Vortex Lattice Methods, and Computational Fluid Dynamics (CFD). In [15] and [16], a strip theory approach is described which uses steady aerodynamic trim forces in addition to the modal data of the structural model to compute the neglected unsteady aerodynamic forces and include them in the flutter process. This method is used herein and referred to as ‘AiM’. The gain in accuracy for flutter point prediction in relation to the conventional DLM approach (referred to as ‘ZONA6’) is compared to linearized frequency domain CFD data (referred to as ‘TAU-LFD’).

The mass and stiffness properties of the structural model are taken from [16]. Two mode shapes are used for the flutter assessment, namely a VTP out-of-plane bending mode with an eigenfrequency of 2.9 Hz and a VTP torsion mode with an eigen-frequency of 5.3 Hz.

Figure 11: Generic T-tail configuration according to [16].

Fig. 12 shows a comparison of the damping curves of the VTP torsion mode (Mode 2) computed by solving the g-method flutter equation with unsteady aerodynamic forces generated by a ZONA6, the AiM method, and TAU-LFD. In this figure, the dimensionless damping coefficient of the second mode shape is displayed against the onset velocity for non-matched flutter computations at Mach numbers of 0.4 (solid lines) and 0.69 (dashed lines).

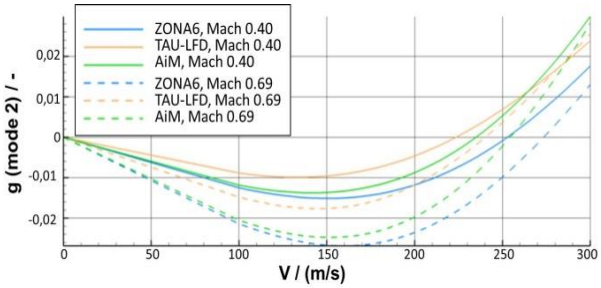

Figure 12: Comparison of damping curves (Mode 2) between ZONA6, TAU-LFD, and AiM at Mach numbers of 0.40 and 0.69.

The AiM method significantly alters the potential flow theory based flutter velocities of the generic T-tail at both Mach numbers. By superposing the DLM forces with the usually neglected aerodynamic forces, the deviations in flutter velocities w.r.t. the CFD based approach can be reduced from 13% to 5-6% for both Mach numbers. Further results and a discussion of the selected approach are published in [11].

3. Common Experimental Means

The XDC part related to experimental means mainly contains the improvement of advanced testing tools related to aerodynamics, vibroacoustics, aeroacoustics and aeroelastics. Besides the development of novel MEMS based high frequency pressure sensors and denoising methods for wind tunnel measurements, optical measurement techniques for accurate flow field investigations, sound source localization methods, contactless deformation measurement techniques as well as instrumentation for vibration testing, are further improved.

The latter four methods are presented briefly in the following.

3.1. Flow Field Measurements

Shake-the-Box (STB) is a novel time-resolved 3D Lagrangian Particle Tracking (LPT) scheme [31] which is suitable for the evaluation of time-series of dense tracer particle images captured from few projections of a laser or LED illuminated measurement volume inside the investigated flow. Dense volumetric tracking of particles over many time-steps allows for accurate time-resolved 3D flow field measurements as it provides position, velocity and acceleration along all reconstructed particle trajectories in the measurement volume. Velocity and acceleration are gained from first and second temporal derivatives of an optimal filtered 3rd order B-Splines as fitting function [34]. Due to the high positional accuracy and large amount of tracks from STB measurements mean flow statistics and Reynolds stresses can be determined with a simple bin-averaging approach delivering a grid or profile of converged data down to sub-pixel resolution [32; 35]. Further on, instantaneous velocity and pressure fields can be efficiently assimilated in a continuous representation by a grid of cubic B-Splines using the scattered particles information as input for solving an inverse, non-linear optimization problem with Navier-Stokes-constraints computed by FlowFit [34]. The analytical spatial derivatives of the velocity and pressure fields can be sampled arbitrarily and provide the whole velocity gradient tensor and pressure hessian with an increased spatial resolution with respect to the mean particle distance (or to former low-pass filtering cross-correlation methods e.g. tomo PIV). The method has been adapted for measurements in high-speed flows using multi-pulse illumination and recording on double-frame images in order to transfer the successful STB tracking methodology to industrial applications, called Multi-pulse STB (MP-STB) [35]. Several successful experimental investigations from low speed laboratory scale up to high-speed industrial and even transonic wind tunnel applications have proven the applicability of both STB methods. As strong shear flows close to surfaces are not a principle problem for such 3D LPT schemes because many individual tracer particles with ~1 µm diameter can be tracked with typical position accuracies < 2 µm in relatively thin wall-parallel measurement volumes, transitional and turbulent boundary layer flows are ideally suited as topics of further investigation.

The extent of laminar flow on aerodynamic surfaces, e.g. swept wings, horizontal and vertical tail planes, with a leading edge sweep larger than 15° is limited by the crossflow instability [24]. The combination of turbulence level and surface structure close to the attachment line determines the dominating crossflow instability mode, i.e., dominating traveling or stationary crossflow modes [21]. For cruise flight conditions, stationary crossflow modes are typically dominant [22, 23].

These stationary crossflow modes were measured in flight with a spanwise wavelength λ in the range from 2 mm to 5 mm [24, 25].

Co-rotating vortices at a fix location with respect to the model surface inside the laminar boundary layer characterize the stationary crossflow instability. After the initial exponential growth of the stationary crossflow vortices, their growth saturates upstream of the transition location. The transition starts with a high-frequency, i.e. typically in the kHz regime, secondary instability at characteristic locations inside of the crossflow vortices [26]. In wind tunnel experiments the 'z'-mode, which is located on the upwelling side of the vortex and at mid height of the boundary layer, were mostly observed [27]. The secondary instabilities grow rapidly and lead to local beginning of turbulent, wedge shaped flow. The goal of the STB experiments is to demonstrate the capability to investigate stationary crossflow instabilities in a relatively thin boundary layer with significant boundary-layer edge velocities, representing a step towards boundary-layer measurements at technically relevant Reynolds numbers.

The experiments to validate the STB will be performed in the "1 Meter Wind Tunnel Goettingen" (1 m-WT), which is a low speed ($U_\infty \leq 70$ m/s) atmospheric wind tunnel of the Göttingen type. The open test section is 1 m wide, 0.74 m high, and 2.4 m long.

At DLR the SPECTRA (Swept flat PlatE Crossflow TRAnsition) experiment [28] was designed to specifically investigate stationary crossflow instability. The model design is based on the design of Bippes and co-workers [22]. As shown in Fig. 13, the model consists of a flat plate with a geometric sweep angle of 45° and a displacement body with a slat to imprint a favorable pressure gradient on the flat plate surface. This design helps to isolate the crossflow instability from other instability mechanisms of a swept wing.

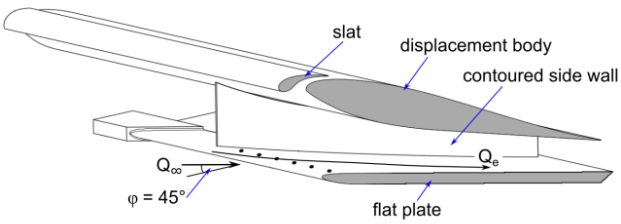

Figure 13: Schematic view of the DLR SPECTRA experiment.

Compared to the original design the SPECTRA experiment has an increased model chord of 0.6 m and a redesigned displacement body shape to avoid flow separation. Contoured side walls help to create infinite swept wing conditions. Discrete roughness elements (DRE) are placed close to the leading edge to achieve a stationary crossflow instability induced transition. These DRE with a diameter of a few millimetres and a height of a few micrometres are placed parallel to the leading edge at a spanwise spacing which corresponds to the most amplified stationary crossflow wavelength of the set-up.

The model part under investigation, i.e., the flat plate, is without curvature and therefore beneficial for volumetric boundary layer measurements with MP-STB.

The MP-STB technique [35] for 3D LPT can be enhanced by using six instead of four successive laser pulses when using frame optimized CCD cameras (FOX) [33]. FOX cams have the ability to capture three frames in short succession by an electronically redesigned sensor charge storage and image read-out strategy. Together with six pulsed Nd:YAG lasers for illumination of small tracer particles in the measurement volume an adapted MP-STB particle tracking technique can be applied to the above described transitional boundary layer flow of the SPETCRA experiment. In the planned experiment within the 1 m-WT of DLR in Goettingen six triple-shutter FOX CCD cameras with 4 Megapixel resolution each will be used (see set-up sketch in Fig. 14) in order to measure ~50,000 individual particle trajectories instantaneously in a laser illuminated volume of ~ 30 x 40 x 5 mm³ in streamwise, spanwise and wall-normal directions close to the wall by MP-STB. A thin glass window inside the flat plate provides optical access for 100 x 175 mm² from below. The cameras will view through this window in a preferable viewing configuration enabling forward light scattering of the particles inside the flow as the collimated laser beam is adjusted to be back-reflected by 180° through the same measurement volume by a mirror and shaped by a passe-partout in order to reduce stray light at the boundaries of the measurement volume. The adapted six-pulse STB particle tracking technique allows reconstructing even longer particle trajectories > 100 pixel (and consequently estimating the particles instantaneous position, velocity and acceleration with higher accuracy in comparison to a four laser pulse strategy). Measuring the spatial and temporal development of flow structures and the related instantaneous skin friction velocity distribution inside a transitional boundary layer flow requires a 3D flow measurement technique with very high dynamic velocity ranges and high spatial resolution. These requirements are fulfilled with the newly adapted MP-STB system. Depending on the availability of a powerful high-repetition rate laser enabling particle illumination and imaging frame rates up ~50 kHz a time-resolved STB measurement set-up with four available v2640 Phantom cameras could be an alternative configuration.

The MP-STB measurements will be supplemented by qualitative skin friction visualization with the Temperature-Sensitive Paint (TSP) method [29].

These visualizations provide a transition location over a large area and also the footprint of stationary crossflow vortices, which provides relative information about the vortex strength [30]. For the SPECTRA experiment the TSP equipment, which consists of four 1.56 Megapixel cameras and five high power LEDs, is integrated in the displacement body, as shown in Fig. 14. The TSP coating is coated into a pocket on the flat plate downstream of the PIV window.

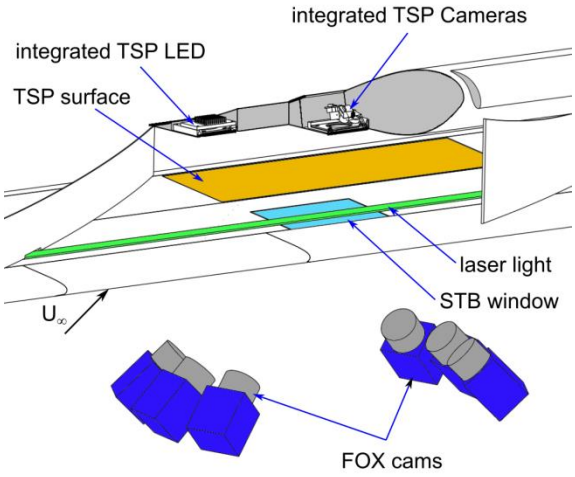

Figure 14: Schematic view of the experimental set-up, i.e., an adapted MP-STB measurement set-up with 6 triple-frame FOX cameras and an integrated TSP set-up, in the DLR SPECTRA experiment at 1m-WT Goettingen.

3.2. Sound Source Localization

Aeroacoustic measurements with microphone arrays for outdoor static engine tests, wind-tunnel tests and aircraft fly-over tests with full-size aircraft are being improved with a focus on the post processing methods.

Figure 15: The DLR ATRA passing over a microphone array (Photo: DLR).

The capability of measuring the amplitudes of individual sources on an aircraft in flight is important for the development of new low-noise aircraft configurations and components. Wind tunnel measurements and numerical calculations struggle with model fidelity, resolution and dynamic range.

For fly-over tests, large microphone arrays with, typically, 240 microphones arranged in multi-arm logarithmic spirals covering an area of 35 by 40 m are laid out on the ground (see Fig. 15). By synchronizing the array data with the GPS trajectory of the aircraft, the positions and amplitudes of the sound sources on the aircraft can be determined using a classical beamforming algorithm for moving sources with a deconvolution of the results with the point-spread-function of the array. This allows to calculate sound source maps as shown in Fig. 16 and Fig. 17. The source amplitudes of individual source regions can be integrated and averaged over several fly-overs. This way, different flight configurations, e.g. take off and climb shown in Fig. 18, or different modifications to the aircraft can be quantitatively compared and evaluated.

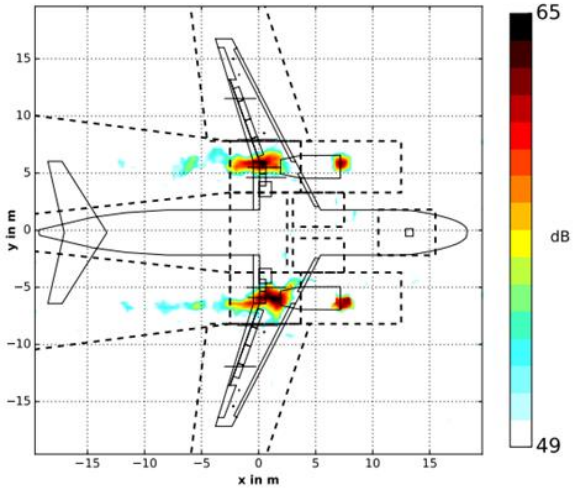

Figure 16: Sound source maps in the 1 kHz band in the forward direction (60°) for a take-off.

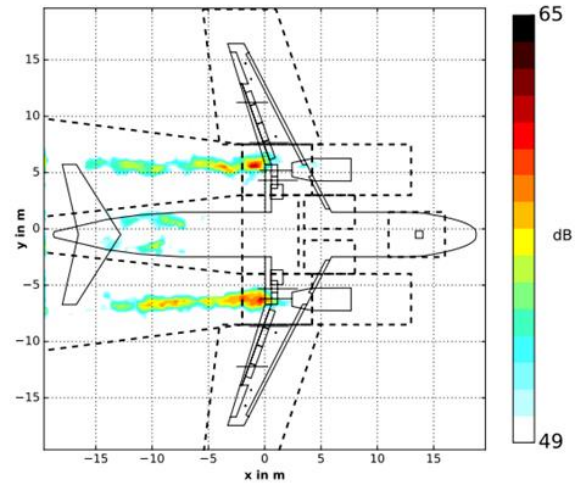

Figure 17: Sound source maps in the 1 kHz band in the rearward direction (120°) for a take-off.

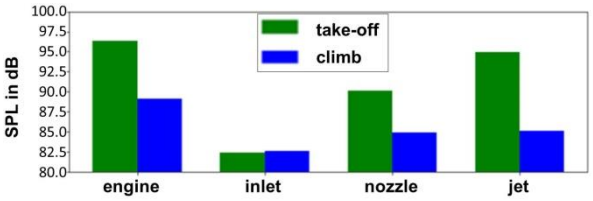

Figure 18: Overall sound pressure of the engine source components for a take-off and a climb configuration in the rear of the aircraft at 120°.

Static noise tests of full-scale engines are required to evaluate new low-noise engine technologies. In this context, DLR developed the source localization method SODIX that determines the amplitudes and the directivities of sound sources. A common setup for a source localization with SODIX at static engine noise tests consists of a large linear microphone array with up to 250 microphones, see Fig. 19.

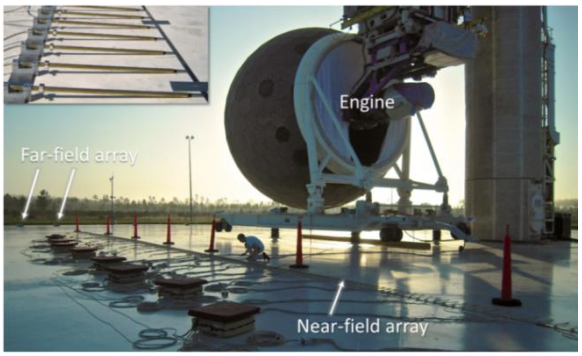

Figure 19: Measurement setup at static engine tests [38].

SODIX fits a model of the cross-spectral matrix to the measured microphone signals and is able to determine the amplitude and the directivity of a set of equivalent sound sources along the engine centerline with high resolution and dynamic range. Fig. 20 shows an example plot of localization results with the axial source position on the horizontal axis and the emission angle on the vertical axis. Sources radiating from the intake, the nozzle, and the jet are clearly separable and the source distribution has a dynamic range of more than 20 dB.

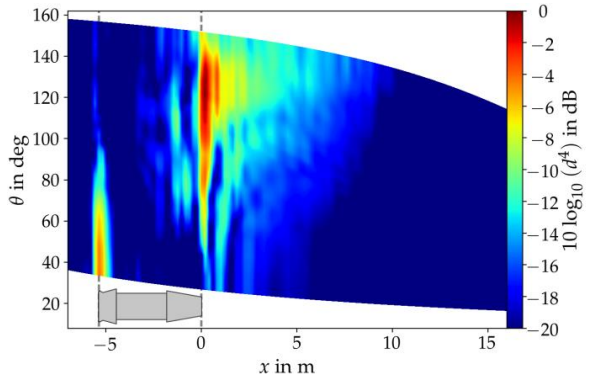

Figure 20: Source localization map derived with SODIX for a turbofan engine [38].

The directive source amplitudes in specific areas, such as the intake, the nozzle, and the jet, can be separated, integrated, and extrapolated to reference positions in the far-field. , Corrections for the atmospheric conditions can also be applied. Fig. 21 shows an example result of the individual spectra of the intake, casing, nozzle, and the jet, which were derived by a geometric source breakdown from the SODIX source maps and an extrapolation to the far-field. The overall sound pressure level derived with SODIX (solid black line) - which is a sum of the individual source areas - agrees well with reference data measured in the far-field (black circles).

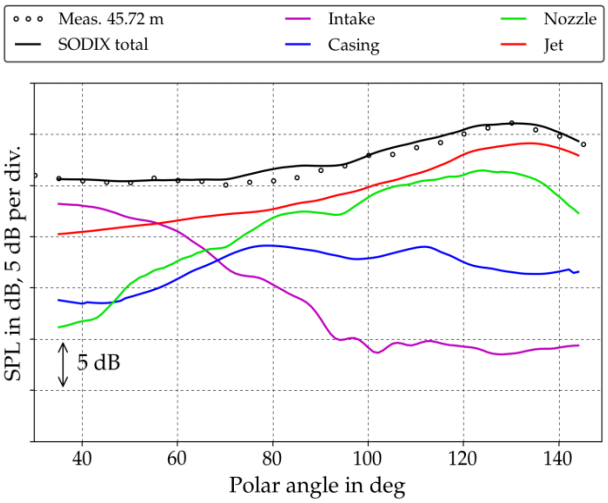

Figure 21: Far-field extrapolation of the localization results derived with SODIX. [38]

The SODIX method has also been applied to a microphone array in the far-field that consists of only 31 microphones. The sparsely populated far-field array is commonly available at static engine test and promises a reduction of computational time and complexity of the microphone setup.

In general, the SODIX method is useful 1) to quantify the contribution of individual components of the engine to the overall noise, and 2) to quantitatively compare different engine configurations, e.g. with and without acoustic treatment.

3.3. Contactless Deformation Measurements

As far as the blade deformation on an OR engine or a large fan is an important parameter to be known, experimental means for non-intrusive deformation measurements are developed and matured within XDC. Especially optical deformation measurement methods (e.g. Image Pattern Correlation Technique (IPCT) [39]) are promising to perform such non-intrusive deformation measurements on full scale ground [40] and flight [41] tests as well as for large scale wind tunnel experiments. An improved IPCT process for blade deformation measurements will be made available within XDC.

3.3.1. IPCT Measurement Setup

The IPCT is a digital image correlation (DIC) method using stereoscopic images of a randomly patterned surface for 3D shape and deformation measurement.

A blade deformation measurement is a special challenge for both the design of a measurement set-up and the evaluation. The measurement set-up can be subdivided into the camera system and the pattern application. In principle there are two possibilities to install a camera system for blade deformation measurement on fast rotating object:

- Non-rotating camera system installed beside the rotor [39,42]
- Rotating camera system installed on the rotor head [40,41]

The first option enables the usage of standard camera systems and the optimization of the set-up with respect to stereo and view angle is much easier than for a rotating the system especially for ground and wind tunnel tests. For the most applications the implementation of a non-rotating camera system is much easier than for a rotating one. A rotating system has to withstand the centrifugal forces and must be well balanced which requires much more effort for a specific compact design of the camera system. Hence its design is strongly limited in the camera base distance and the installation height of the cameras over the observed surface. The resulting very small stereo - and flat viewing angles can complicate the evaluation and reduce the accuracy of the measurement system.

On the other hand a rotating system enables a 360° phase measurement and avoids the problem of motion blur. Non- rotating systems can often cover only a small phase angle section by a single setup. Additionally they require strong illumination sources like laser or high-power LED arrays to permit the short exposure times which are necessary to avoid motion blur. Within the XDC High-Power LEDs in pulsed operation mode were tested successfully for a propeller blade deformation. They illuminated an area of approximately 500 x 300 mm² with 2 µs light pulses to freeze the blade position of a fast rotating propeller.

Also for the pattern application there are two approaches:

- Surface fixed pattern
- Space fixed projected pattern

The standard procedure to apply a fixed pattern onto a blade with a strong 3D-curvature is painting using a stencil [41]. For composite blades it was tested to apply the pattern within the manufacturing process successfully. Therefore the IPCT pattern was transferred by means of a stencil to the mould. Fig. 21 shows a composite specimen.

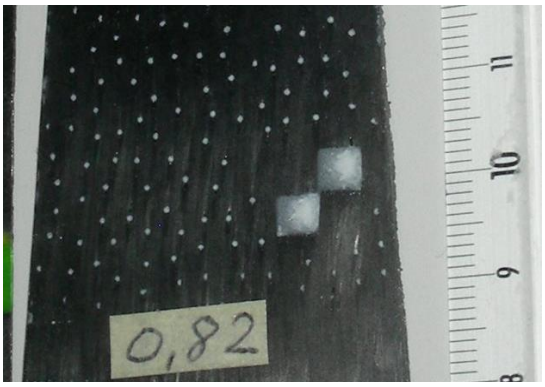

Figure 21: Composite specimen with correlation pattern and marker applied within the manufacturing process.

If the application of a fixed pattern is not feasible it can be projected onto the surface, but it must be considered, that the contrast of the projected pattern depends strongly from the background. Fig. 22 demonstrates the remarkable influence of the background properties by means of a blade deformation measurement [42]. Three of the nine propeller blades were prepared for a TSP/PSP measurement: blade 3, 4 and 5 were varnished with a white primer and blade 4 and 5 were additionally covered with TSP or PSP respectively. A pattern was projected by means of a pulsed laser to the propeller blades. Fig. 4 b) and c) show the sample images of an IPCT-camera at different phase positions of the propeller. The unprepared black blades reflect not sufficient light for an IPCT – evaluation whereas the painted blades deliver a very good signal. Finally for this IPCT application on composite blades a preparation of the blade surface was necessary for the projected pattern method as well. For a fan blade deformation measurement on a V2500 engine of an Airbus A320 in ground operation the pattern was projected direct to the fan by means of a pulsed ND-YAG laser [43]. The metallic fan surface has a higher reflectivity but with a directional dependency which have to be considered in the placement of the cameras and light source with respect to the surface normal.

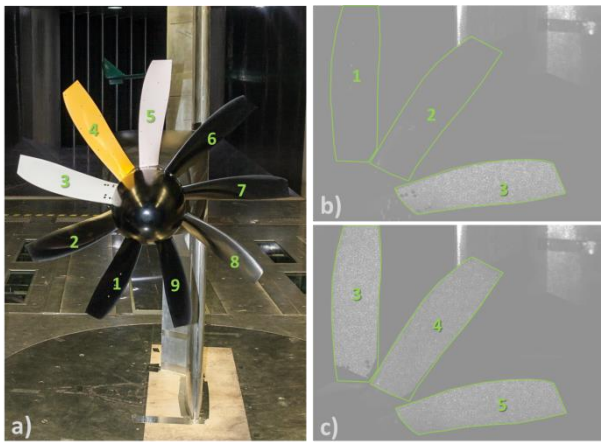

Figure 22: Pattern projected on a propeller by means of a laser on differently prepared surfaces

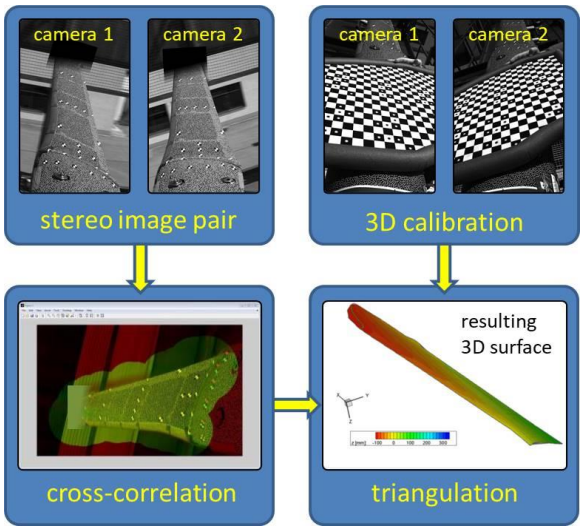

Figure 23: Scheme of the IPCT evaluation.

3.3.2. IPCT evaluation

The simplified IPCT processing for a 3D surface measurement is shown in Fig. 23. The stereoscopic image pair is cross-correlated in order to find corresponding pattern regions in the stereo views. To obtain the measured 3D surface the image coordinates of the corresponding points (CPs) are triangulated using a 3D camera calibration.

For a 3D deformation measurement the IPCT processing was extended by a time series correlation part. Instead of correlating the images of two cameras at the same time, the image correlation is performed here between the reference state and the measurement state for both stereo views respectively. Linking the point correspondences of the time series correlation with the CPs between the stereo views of the reference the new 3D position of the reference grid points can be calculated and a 3D displacement vector field is determined by subtraction. The time series correlation is only applicable for a surface fixed pattern.

Strong loads and vibrations can lead to a movement of the cameras with respect to the measurement object as well as between the cameras which leads to a decalibration of the camera system. Additionally an offset in the position of the measurement object between reference and measurement state is possible. Thus these effects have to be corrected in a further post-processing to deduce the correct wanted deformation from the measured displacement.

A recalibration method [44] was developed to correct a movement between the cameras. The method was further refined to cope with very small stereo angles and tested for large displacement in laboratory successfully.

Fig. 24 shows a laboratory set up where a camera decalibration was simulated by a shift of one camera (cam2) by 150 mm.

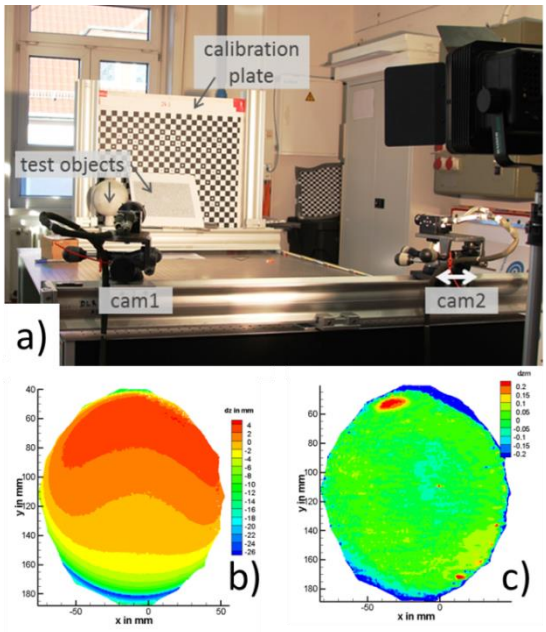

Figure 24: Laboratory test of recalibration procedure: a) set-up, b) dz calculated with decalibrated camera parameters , c) dz calculated with recalibrated camera parameters.

Fig. 24 b) and c) show for the test sample of a sphere the deviation dz of the measured surface to an ideal sphere, which was fitted to the measured point cloud. The sphere fitted to the results of the decalibrated set up had a radius of 70.6 mm (nominal radius 80 mm) and the deviation dz is in a range of $-26 < dz < 4$ whereas after the recalibration the radius of the fitted sphere was 79.9 mm with $-0.2 < dz < 0.2$, which is consistent to the accuracy of the set-up.

Further post-processing routines were developed to use the time-series correlation for the mapping of different stereo camera systems with an overlapping area as well as for the calculation of Rigid Body Transformations (RBT). For both cases the RBT is determined by a minimisation of the displacement of a selected area between two stereo systems or two states respectively.

The optimisation of a measurement set-up to determine blade deformations on fast rotating propellers is often quite limited by different constraints, like optical access, loads, safety issues. The improvements of the evaluation tools and the enhanced post-processing tools of the IPCT developed and tested within XDC facilitate not only standard application but enable also an IPCT evaluation even for bad conditioned measurement set-ups and enlarge the scope of application of the technique.

3.4. Vibroacoustics

Acoustic comfort for large passenger aircrafts has become a particularly important topic in the last decades. In order to provide design decisions that help to minimize cabin noise, it is necessary to fully

understand the source generation mechanisms and the transmission paths involved. The study of such problem presents a great challenge, since any experimental analysis will require numerous flight tests for data acquisition and evaluation, which means extremely high costs for research and development. If we consider that one of the most important sources of cabin noise in the low-middle frequency range are the engines, our contribution consist in the development of an active excitation system that will mimic the vibrational behaviour of those engines. This will help to facilitate the vibroacoustic research by allowing to replace flight tests by ground or laboratory tests.

The developed system should be able to mimic the three-dimensional forces and moments, as depicted in Fig. 25, introduced by a real engine into an arbitrary structure, a demonstrator structure or a real wing if necessary. The system is based on a multichannel active controller. Such system takes as input a reference model that represents the behaviour of the engine and generates the control signals that are fed to the force actuators that drive the vibratory response. The moments are generated in a similar way, except for the fact that a pair of opposite forces on an attachment device is used.

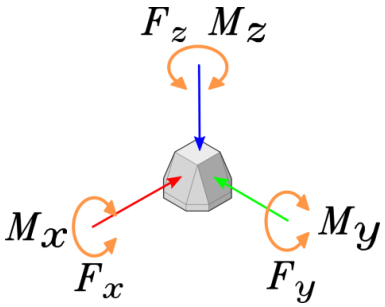

Figure 25: Schematics of forces Fxyz and moments Mxyz that the active system will control.

The control system has been developed gradually; first, a simple proof of concept was realized with a single-input single-output (SISO) force controller. Next, a multi-input multi-output (MIMO) system was able to control the injected forces in the three directions of space. Later a multi-input single-output MISO moment control system was developed. All these incremental steps have being described and reported in numerous publications [45 - 48].

In order to exemplify the work already performed, two cases are shown, the first one describes the performance of the MIMO force controller and the second one presents the MISO moment controller. The test structure used was a single aluminium plate of 1 x 0.8 x 0.03 m, with an asymmetric milled pattern that resembles the skin fields, stringers and frames typically found in fuselage structures. The thickness of the skin fields, stringers and frames was 1, 5 and 10 mm respectively. The plate was suspended using bungee cords in order to generate free displacement boundary conditions, as seen in Fig. 26.

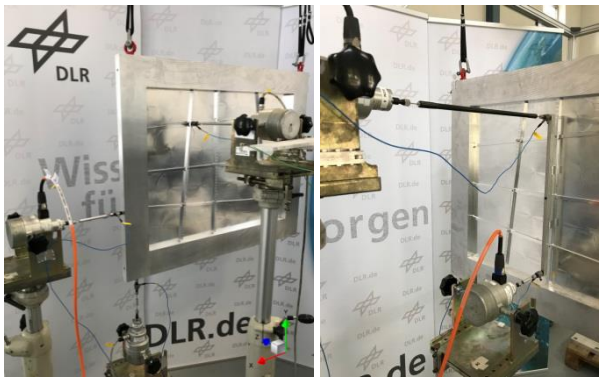

Figure 26: Aluminium plate configuration for force control (left) and for moment of force control (right).

For the evaluation of the MIMO force control implementation, three shakers are attached, one per spatial direction as seen in Fig. 26 left. In this case, three different frequency profiles were arbitrarily defined. These profiles serve as the target reference that the controller will try to replicate at the injection point of the structure. The result of the evaluation is summarized in Fig. 27, where the Reference profiles and the Control ON conditions are shown. There, each colour represents one direction in space, the solid and dashed lines represent the Reference and the Control ON respectively.

From Fig. 27 it is possible to establish the correct operation of the controller. The good agreement among references and resulting profiles illustrates the proper generation of control forces.

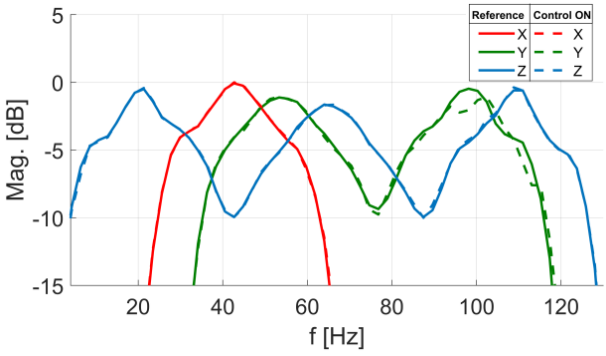

Figure 27: Spectral comparison of Force control, References vs. Control ON condition.

The evaluation of the MISO moment controller is performed in the same way as in the previous case, where the frequency Reference model is compared against the actual moment generated by the Control ON condition. The result is shown in Fig. 28. There it is possible to notice the relatively good agreement between both curves, which means that the controller is properly generating the correct moment at the center point between applied forces.

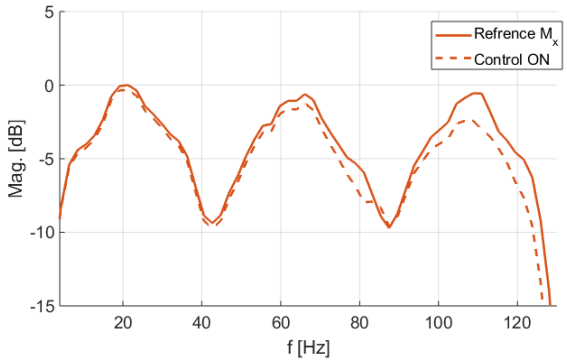

Figure 28: Spectral comparison of Moment M_x control, Reference vs. Control ON.

In future work, it is planned to integrate the two main parts of the control system, i.e. forces and moments, into a single global controller in order to achieve the original goal of our proposed system. Such development will help in the future to easily perform laboratory experiments that will replicate the vibroacoustic behaviour of an engine, enabling to carry out noise cabin research in a more accessible way.

4. Conclusions and Summary

The paper presents some of the developments in the LPA Platform 1 XDC demonstrator in the field of numerical simulation tools and experimental methods.

The presented work related to numerical aerodynamic simulations demonstrated the capabilities of modern CFD methods, like the DLR TAU Code, in delivering highly accurate performance predictions for future propulsion systems and details of the complex engine aerodynamics. These capabilities will be valuable for the assessment of the benefits and challenges of highly integrated propulsion systems.

Another important issue addressed in the paper was the prediction of the noise impact of integrated engine concepts resulting from aeroacoustic effects. It has been shown that some aspects e.g. related to UHBR engines can be solved by using analytical methods like the PropNoise approach. The application of such tools will support the preliminary design process by an easy assessment of the acoustic impact even in an early stage when detailed information about the aerodynamics is not yet available.

With respect to aeroelastic stability analysis representative reference models have been created that now can be used for aeroelastic analysis, loads analysis and vibroacoustic analysis for engine integration studies. Furthermore the AiM method for T-tail stability analyses has been tested successfully.

Besides the developments of numerical method, also advanced experimental means like the non-intrusive optical measurement techniques for flow fields (i.e. STB) and deformation (i.e. IPCT) are improved within the project. For the demonstration of the STB method, that is able to deliver time-resolved 3D flow field data and pressure fields, a validation experiment, related to the investigation of stationary crossflow instabilities in a relatively thin boundary layer, is being prepared. As a supplement to the STB measurement qualitative skin fraction measurements by means of TSP are performed using a model integrated illumination and camera installation. The lessons learnt from the camera integration will be beneficial for future application of optical methods to areas with difficult optical access. In the scope of future research projects it is foreseen to apply the STB and MP-STB techniques to BLI investigations, engine inlet flows, BL fan interaction, aero acoustic noise source investigations, and for the generation of spatially well resolved validation data for CFD methods and the development of advanced turbulence models (e.g. DRSM).

The non-intrusive shape and deformation measurement technique IPCT has been improved further in order to deliver surface deformation time series and to be able to cope with small unwanted camera movements. The IPCT method thus becomes a more and more robust measurement technique even for bad conditioned measurement set-ups.

Source localisation methods for static engine tests and aircraft in flight are being improved and prepared for application in the measurement campaigns for the demonstrators. These methods provide information on the location and the amplitudes of the different source regions of aircraft and engines in wind-tunnel, static and fly-over tests.

In the field of vibroacoustics an active excitation system replicating the vibrational behaviour of engines is being developed. This system will help to reduce the amount of flight test activities for cabin noise research.

Besides the activities presented in this paper several different achievements have been made within the project and more will follow within the next years until the end of the project duration. All together those activities and achievements will help to better understand advanced propulsion concepts and optimize their integration in the airframe.

5. Acknowledgement

The authors would like to thank all helping hands that enable the performance of the work presented in this paper. This project has received funding from the Clean Sky 2 Joint Undertaking under the European Union's Horizon 2020 research and innovation programme under the grant agreement Number 807097 - LPA GAM 2018 - H2020 – IBA - CS2 - GAMS - 2017.

6. REFERENCES

1. Laban, M.; Kok, J.; Brouwer, H. (2018). CFD/CAA Analysis of UHBR Engine Tonal Noise. *Proceedings of the AIAA Aviation 2018*, Atlanta, GA, USA, 25–29 June 2018; AIAA 2018-3780.
2. Burlot, A.; Sartor, F.; Vergez, M.; Meheut, M.; Barrier, R. (2018). Method Comparison for Fan Performance in Short Intake Nacelle. *Proceedings of the AIAA Aviation 2018*, Atlanta, GA, USA, 25–29 June 2018; AIAA 2018-4204.
3. Peters, A.; Spakovszky, Z.S.; Lord, W.K.; Rose, B. (2014). Ultrashort Nacelles for Low Fan Pressure Ratio Propulsors. *J. Turbomach. 2014*, 137, 021001.10.1115/1.4028235
4. Thollet, W.; Dufour, G.; Carbonneau, X.; Blanc, F. (2016). Body-force modeling for aerodynamic analysis of air intake-fan interactions. *Int. J. Numer. Methods Heat Fluid Flow 2016*, 26, 2048–2065.10.1108/HFF-07-2015-0274.
5. Akaydin, H.D.; Pandya, S.A. (2017). Implementation of a Body Force Model in OVERFLOW for Propulsor Simulations. *Proceedings of the 35th AIAA Applied Aerodynamics Conference*, Denver, CO, USA, 5–9 June 2017; doi:10.2514/6.2017-3572.
6. Hall, D. K., Greitzer, E. M.; Tan, C. S. (2017). Analysis of Fan Stage Conceptual Design Attributes for Boundary Layer Ingestion. *J. Turbomach. 2017*, 139, 071012.10.1115/1.4035631.
7. Stuermer, A. (2019). DLR TAU-Code uRANS Turbofan Modeling for Aircraft Aerodynamics Investigations. *Aerospace 2019*, 6, 121.
8. Schnell, R., Goldhahn, E., Julian, M. (2019). Design and Performance of a Low Fan-Pressure-Ratio Propulsion System. *Proceedings of the 25th International Symposium on Air Breathing Engines ISABE 2019*, Canberra, Australia, 22–27 September 2019; Number ISABE-2019-24017.
9. Moreau, Staggat, Gscheidle (2019). A fast prediction method for rotor buzz-saw noise based on an analytical approach. *25th AIAA/CEAS Aeroacoustics Conference*, Delft, paper N° AIAA-2019-2641, 2019.
10. Moreau, Guérin (2020). Experimental Validation of an analytical prediction model for fan buzz-saw noise. *ASME Turbo Expo Conference*, London, paper N° GT2020-14279, 2020.
11. Schäfer, D., Arnold, J. (2019). Assessment of T-Tail Flutter Using an Enhanced Potential Flow Theory Approach and Linearized Frequency Domain CFD Data. *International Conference on Aeroelasticity and Structural Dynamics (IFASD)*, Savannah, June 2019.
12. Handojo, V., Lancelot, P., De Breuker, R. (2018). Implementation of Active and Passive Loads Alleviation Methods on a Generic Mid-Range Aircraft Configuration. *AIAA Aviation Forum*, 2018.
13. Klimmek, T., Schulze, M., Abu-Zurayk, M., Ilic, C., Merle, A. (2019). cpacs-MONA – An independent and in high fidelity based MDO tasks integrated process for the structural and aeroelastic design for aircraft configurations. *IFASD 2019 - International Forum on Aeroelasticity and Structural Dynamics*, 10.-13. Juni 2019, Savannah, GA (USA).
14. Klimmek, T. (2014). Parametric Set-Up of a Structural Model for FERMAT Configuration for Aeroelastic and Loads Analysis. *Journal of Aeroelasticity and Structural Dynamics*, 3 (2), pp 31-49. Department of Aerospace Engineering of Politecnico di Milano.
15. Jennings, W., Berry, M. (1977). Effect of Stabilizer Dihedral and Static Lift on T-Tail Flutter. *Journal of Aircraft*, pp. 364-367, 1977.
16. Murua, J., van Zyl, L., Palacios, R. (2014). T-Tail flutter: Potential-flow modelling, experimental validation and flight tests. *Progress in Aerospace Sciences*, pp. 54-84, 2014.
17. van Zyl, L., Mathews, E. H. (2011). Aeroelastic Analysis of T-Tails Using an Enhanced Doublet Lattice Method. *Journal of Aircraft*, vol. 48, pp. 823-831, 5 2011.
18. Suciu, E. (1996). MSC/Nastran Flutter Analyses of T-Tails Including Horizontal Stabilizer Static Lift Effects and T-Tail Transonic Dip.
19. McCue, D. J., Gray, R., Drane, D. A.(1971). The Effect of Steady Tailplane Lift on the Subcritical Response of a Subsonic T-Tail Flutter Model.
20. Schrauf, G. (2005). Status and perspectives of laminar flow, *Aeronaut. J.* 109 (2005) 639–644, doi.org/10.1017/S000192400000097X
21. Hunt, L., Saric, W. (2011). Boundary-layer receptivity of three-dimensional roughness arrays on a swept-wing, *41st AIAA Fluid Dynamics Conference and Exhibit*, 27–30 June 2011, Honolulu, Hawaii, AIAA 2011-3881, 2011, https://doi.org/10.2514/6.2011-3881
22. Bippes, H. (1999). Basic experiments on transition in three-dimensional boundary layers dominated by crossflow instability, *Prog. Aerosp. Sci. 35* (1999) 363–412, https://doi.org/10.1016/S0031-8914(53)80099-6
23. Saric, W., Reed, H., White, E. (2003). Stability and transition of three-dimensional boundary layers. *Annu. Rev. Fluid Mech. 35* (2003) 413–440, https://doi.org/10.1146/annurev.fluid.35.101101.161045
24. Schrauf, G., Perraud, J., Vitiello, D., Lam, F. (1998). Comparison of boundary-layer transition predictions using flight test data. *J. Aircraft 35* (1998) 891–897, https://doi.org/10.2514/2.2409
25. Herbert, T., Schrauf, G. (1996). Crossflow-dominated transition in flight tests. *34th Aerospace Sciences Meeting and Exhibit*, 15–18 January 1996, Reno, Nevada, AIAA 96-0185, 1996, https://doi.org/10.2514/6.1996-185
26. Kohama, Y., Saric, W., Hoos, J. (1991). A high-frequency, secondary instability of crossflow vortices that leads to transition. *Proc. R. Aerosp. Soc. Conf. Bound.-Layer Transit. Control Conf.* Peterhouse College, Cambridge, UK, 1991, pp. 4.1–4.13
27. Wassermann, P., Kloker, M. (2002). Mechanisms and passive control of crossflow-vortex induced transition in a three-dimensional boundary layer. *J. Fluid Mech. 456* (2002) 49–84,

https://doi.org/10.1017/S0022112001007418

28. Barth, H. P.; Hein, S.; Rosemann, H. (2017). Redesigned Swept Flat-Plate Experiment for Crossflow-Induced Transition Studies. *Notes on Numerical Fluid Mechanics and Multidisciplinary Design*, Springer International Publishing, 2017 , 155-165

29. Liu, T., Sullivan, J. P. (2005). *Pressure and Temperature Sensitive Paints*, Springer-Verlag, 2005

30. Lemarechal, J., Costantini, M., Klein, C., Kloker, M. J., Würz, W., Kurz, H. B. E., Streit, T., Schaber, S.(2019). Investigation of stationary-crossflow-instability induced transition with the temperature-sensitive paint method. *EXP THERM FLUID SCI 109*, 109848.

31. Schanz, D., Gesemann, S., Schröder, A. (2016). Shake-The-Box: Lagrangian particle tracking at high particle image densities, *Exp. Fluids 57:5*

32. Schröder, A., Schanz, D., Geisler, R., Gesemann, S. (2016). Investigations of coherent structures in near-wall turbulence and large wall-shear stress events using Shake-The-Box. *18th Intern. Symp. on Appl. of Laser Techniques to Fluid Mechanics*, Lisbon, Portugal.

33. Geisler R. (2014). A fast double shutter system for CCD image sensors. *Meas Sci Technol 25:025404*

34. Gesemann, S., Huhn, F., Schanz, D., Schröder, A. (2016). From noisy particle tracks to velocity, acceleration and pressure fields using B-splines and penalties. *18th Int. Symp. on Appl. of Laser Techniques to Fluid Mechanics*, Lisbon, Portugal

35. Novara, M., Schanz, D., Geisler, R., Gesemann, S., Voss, C., & Schröder, A. (2019). Multi-exposed recordings for 3D Lagrangian particle tracking with Multi-Pulse Shake-The-Box. *Experiments in Fluids, 60(3)*, 44.

36. Siller, H. (2012). Localisation of sound sources on aircraft in flight. BeBeC-2012-01 in proceedings of the 4th *Berlin Beamforming Conference, 22-23 February 2012.* Gesellschaft zur Förderung angewandter Informatik e. V., Berlin, *ISBN 978-3-942709-04-0*.

37. Michel, U., Funke, S. (2008). Noise source analysis of an aeroengine with a new inverse method SODIX. *14th AIAA/CEAS Aeroacoustics Conference (29th AIAA Aeroacoustics Conference)*, May 5-7, 2008, Vancouver, British Columbia, AIAA 2008-2860. 2008.

38. Oertwig, S., Funke, S., Siller, H. (2018). Improving source localisation with SODIX for a sparse microphone array. BeBeC-2018-S05 in proceedings of the 7th *Berlin Beamforming Conference*, 5-6 March 2018, Gesellschaft zu Förderung angewandter Informatik e. V., Berlin.

39. Kirmse, T., Boden, F. & Jentink, H. (2013). Image pattern correlation technique (IPCT), *AIM² Advanced Flight Testing Workshop - HANDBOOK of ADVANCED IN-FLIGHT MEASUREMENT TECHNIQUES*, ch. 6, 63-85, BoD - Books on Demand, Norderstedt

40. Boden, F., Stasicki, B., Ludwikowski, K. (2018). Optical Rotor-Blade Deformation Measurements using a Rotating Camera System. *ETTC 2018*, 26th to 28th of May 2018, Nürnberg, Germany. DOI: 10.5162/ettc2018/7.4

41. Boden, F., Stasicki, B., Szypuła, M., Ružička, P., Tvrdik, Z. and Ludwikowski, K. (2016). In-flight measurements of propeller blade deformation on a VUT100 cobra aeroplane using a co-rotating camera system. *Measurement Science & Technology, 27 (7),* Institute of Physics (IOP) Publishing. DOI: 10.1088/0957-0233/27/7/074013

42. Roosenboom, E., Geisler, R. und Agocs, J.,Schanz, D., Weikert, T., Kirmse, T., Schröder, A. (2013). Assessment of propeller induced properties and active flow control using multiple image-based measurement systems. *10th International Symposium on Particle Image Velocimetry – PIV13*, 01. - 03. Jul. 2013, Delft, The Netherlands.

43. Kirmse, T., Maring, S., Schröder, A, Ebel, P. B. (2016). Image Based Fan Blade Deformation Measurements on an Airbus A320 V2500 Engine in Ground Operation. *AIAA SciTech 2016*, 04. - 08. Jan. 2016, San Diego, CA, USA. DOI: 0386

44. Kirmse, Tania (2016). Recalibration of a stereoscopic camera system for in-flight wing Deformation measurements*. Measurement Science & Technology, 27 (5),* IOP. DOI: 10.1088/0957-0233/27/5/054001

45. Norambuena, M., Winter, R. (2019). Active structural excitation as known source for structure-borne noise research. *INTER-NOISE 2019*, Madrid, 2019.

46. Norambuena, M., Winter, R. (2019). An adaptive structural excitation system as a tool for structure-borne noise research. *ICA 2019 - 23rd International Congress on Acoustics*, Aachen, 2019.

47. Norambuena, M, Winter, R., Biedermann, J. (2018). Accurate structural excitation through adaptive control. *International Conference on Noise and Vibration Engineering ISMA 2018*, Leuven, 2018.

48. Norambuena, M., Winter, R., Biedermann, J. (2018). Inverse control applied to structural excitation systems. *DAGA 2018 - 44. Jahrestagung für Akustik*, München, 2018.

- **Acknowledgement**

  This project has received funding from the Clean Sky 2 Joint Undertaking (JU) under grant agreement No 807097. The JU receives support from the European Union's Horizon 2020 research and innovation programme and the Clean Sky 2 JU members other than the Union.